Journal of Magnetism and Magnetic Materials 586 (2023) 171186

Contents lists available at ScienceDirect

Journal of Magnetism and Magnetic Materials

journal homepage: www.elsevier.com/locate/jmmm

Research article

Tuning in-plane magnetic anisotropy and temperature stability in amorphous trilayers

Julia Löfstrand[1], Parul Rani[1], Petra E. Jönsson, Gabriella Andersson *

Department of Physics and Astronomy, Uppsala University, Box 516, SE-751 20 Uppsala, Sweden

ARTICLE INFO

Keywords:
Ternary alloys
Thin films
Multilayers
Magnetic properties
Magnetic anisotropy
Curie temperature

ABSTRACT

Better understanding of the nature of magnetic coupling in soft/hard nanocomposites paves the way for tailored exchange-spring magnets. We have investigated a series of amorphous magnetic thin films and trilayers of magnetically soft $Co_{85}(Al_{70}Zr_{30})_{15}$ and magnetically hard $Sm_{12}Co_{81}Ti_7$, produced with DC magnetron sputtering. The overall magnetic properties of the trilayers were investigated with focus on the effects of layer configuration and thicknesses on coercivity, originating from the $Sm_{12}Co_{81}Ti_7$ phase, and uniaxial in-plane anisotropy induced from the $Co_{85}(Al_{70}Zr_{30})_{15}$ phase. In addition, we found that the thermal stability of a 20 nm $Sm_{12}Co_{81}Ti_7$ layer was significantly increased if surrounded by two 10 nm $Co_{85}(Al_{70}Zr_{30})_{15}$ layers in a trilayer structure.

1. Introduction

Artificially layered magnetic systems display a remarkable variety of physical phenomena, with important technological applications in e.g. information processing and storage [1]. For a long time, much effort has been devoted to epitaxial growth and obtaining atomically flat interfaces [2]. However, recently the interest in magnetic materials with graded interfaces is growing [3] and it has e.g. been shown that this intermixing at the interface can improve the magnetic properties of exchange-spring magnets [4]. Exchange-spring magnets consist of combined nanometer-scale hard and soft magnetic phases. They were originally investigated mainly with the purpose of obtaining strong permanent magnets, containing less rare earth elements while still achieving a high energy product [5–8]. For permanent magnets, the goal is to obtain a rigid coupling between the two phases, so that the magnetisation of the entire soft magnetic layer follows the hard magnetic phase. The exchange-spring regime, where the spin orientation in the soft phase is non-uniform instead, is obtained if the thickness of the soft layer is larger than a critical thickness of typically 10 nm [9]. Such exchange-spring magnets are of interest for achieving suitable magnetisation reversal in spintronics applications [10,11].

Amorphous magnetic layered structures can be realised by magnetron sputtering. With this process, smooth interfaces can be achieved, with no crystalline defects or strain from lattice mismatch [12]. The magnetic properties of each layer can be tuned by the composition and the interfaces are naturally graded due to a degree of intermixing occurring as a result of the sputtering process [13,14]. For amorphous alloys with d-electrons responsible for the magnetism, the local anisotropy is to a large extent averaged out, yielding very low coercivity as explained by the random anisotropy model [15,16]. If the film deposition is homogeneous, which can be ensured e.g. by rotating the substrate during sputtering, one could naively expect isotropic in-plane magnetic response. However, uniaxial in-plane magnetic anisotropy is often observed in sputtered amorphous soft-magnetic films [17–21]. This uniaxial anisotropy may have multiple origins. Depending on the properties of the substrate, it has been shown to be due to bond-orientational anisotropy in some studies [18,22] and to magnetoelastic anisotropy from (residual) strain in the film in others [19,20,23]. Having soft magnetic films with a uniaxial anisotropy is important for e.g. spintronic applications, magnetic recording, magnetic sensors and microwave devices and it is also possible to imprint a well-defined uniaxial anisotropy by sputtering in a magnetic field [24,25].

In amorphous alloys with f electrons, e.g. Sm-Co, the random anisotropy strongly affects the interactions, and may give rise to hard magnetic behaviour if the anisotropy is too strong to be averaged out [15,16]. Amorphous Sm-Co films sputtered onto rotating amorphous substrates are typically magnetically isotropic in-plane, but a uniaxial anisotropy can be induced by applying an external magnetic field during deposition [26–28].

In this study, we have investigated trilayer structures with a configuration of either hard/soft/hard or soft/hard/soft amorphous magnetic

* Corresponding author.
E-mail address: gabriella.andersson@physics.uu.se (G. Andersson).
[1] Shared first authorship.

https://doi.org/10.1016/j.jmmm.2023.171186
Received 26 April 2023; Received in revised form 16 August 2023; Accepted 25 August 2023
Available online 28 August 2023

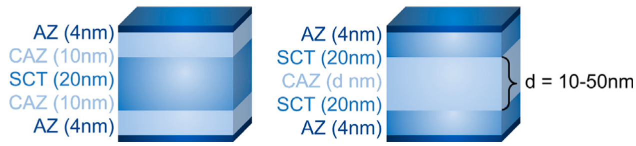

Fig. 1. Illustration of the magnetic trilayer samples with the two possible configurations, with either the magnetically soft $Co_{85}(Al_{70}Zr_{30})_{15}$ (CAZ) or the magnetically hard $Sm_{12}Co_{81}Ti_7$ (SCT) in the centre of the stack. In both cases, buffer and capping layers of $Al_{70}Zr_{30}$ (AZ) enclose the magnetic trilayer. For the configuration with CAZ as the middle layer (right), multiple samples with a range of thicknesses (d) of this layer were produced.

alloys, where the hard and soft magnetic layers consist of $Sm_{12}Co_{81}Ti_7$ and $Co_{85}(Al_{70}Zr_{30})_{15}$, respectively. Both alloys are ferromagnetic at room temperature, but the hard phase has a much lower Curie temperature (T_c) than the soft phase. For these trilayers, we explore the effects of layer configuration and layer thickness on overall anisotropy, coercivity, and saturation magnetisation.

2. Sample fabrication and experimental methods

Thin film samples with amorphous layers of the magnetically soft $Co_{85}(Al_{70}Zr_{30})_{15}$ (CAZ) and magnetically hard $Sm_{12}Co_{81}Ti_7$ (SCT) were grown using DC magnetron sputtering in a non-commercial ultra high vacuum (UHV) system with a base pressure below 10^{-8} Torr (typically in the low 10^{-9} Torr range) [29,30]. Before deposition, Ar gas with a pressure of 2 mTorr was introduced to the sputtering chamber. Highly pure (99.99 at.%) sputtering targets with a 3-inch diameter were used, consisting of an $Al_{70}Zr_{30}$ composite, as well as Co, Sm, and Ti, respectively.

The substrates, single crystalline Si(100) with a native oxide and an area of $\sim 1\,cm^2$, were rotated during deposition at a rotational speed of 20 rpm, to ensure a homogeneous deposition. The sputtering yield of each target was calibrated in order to calculate the sputtering time and power required for the desired thicknesses and compositions. For all samples, 4–5 nm thick layers of $Al_{70}Zr_{30}$ were used as buffer layers to ensure amorphous growth of the following magnetic layer and as capping layers to prevent oxidation of the material underneath [12]. The capping layer becomes naturally oxidised in air, and the resulting 1–2 nm thick layer of self-passivating Al_2O_3 prevents any further oxidation of the sample. The magnetic trilayer samples with the two respective configurations of CAZ/SCT/CAZ and SCT/CAZ/SCT are illustrated in Fig. 1. For the configuration with the magnetically soft alloy at the centre, multiple samples with a range of soft layer thicknesses $d = 10 - 50$ nm were produced and investigated.

To confirm that the chosen sputtering parameters produced X-ray amorphous samples, grazing incidence X-ray diffraction (GI-XRD) was performed on single films of $Co_{85}(Al_{70}Zr_{30})_{15}$ and $Sm_{12}Co_{81}Ti_7$, at 1° incidence for a 2θ range of $10 - 80°$ in a Bruker D5000 system with Cu K_α radiation ($\lambda = 1.5418$ Å). X-ray reflectivity (XRR) was measured in a Bruker D8 Discover system, also with CuK_α radiation, for a 2θ range of $0.2 - 5°$. To extract the information on film thickness, density, and interface roughness, the XRR data was fitted in the software *GenX* [31].

Magnetic hysteresis loops were measured at room temperature in a LakeShore 7404 Vibrating Sample Magnetometer (VSM). The measurements were performed in-plane, in a continuous mode and the sample holder was rotated so that one hysteresis loop was taken at least every 30° for a full 360° rotation in order to investigate the anisotropy. Measurements of angle-dependent hysteresis loops were also performed in a non-commercial Magneto-Optic Kerr Effect (MOKE) system, for higher field resolution. Temperature dependent magnetic measurements were performed in a Quantum Design MPMS SQUID, where the samples were mounted so that the field was applied in-plane, along one of the sample edges.

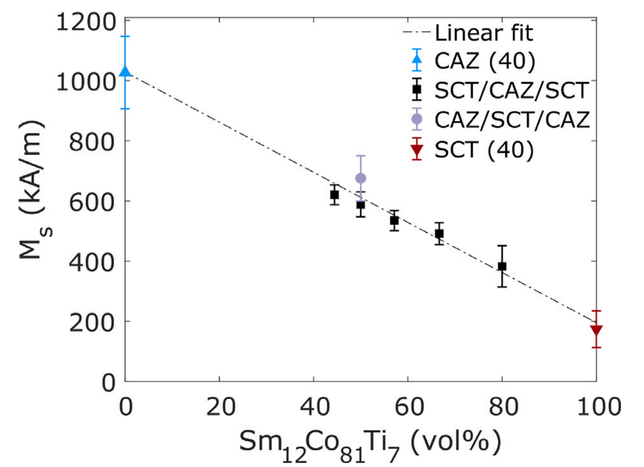

Fig. 2. Room temperature M_s versus relative content (vol.%) of $Sm_{12}Co_{81}Ti_7$ in the full magnetic segment of the film. The M_s values were determined from in-plane $M(H)$ loops measured using VSM. The dashed line shows a linear fit to all data points.

Table 1
Layer thicknesses for the buffer, capping, and magnetic layers, and their corresponding uncertainties, extracted from fits of XRR data using the software *GenX* [31]. The phases $Co_{85}(Al_{70}Zr_{30})_{15}$ (CAZ) and $Sm_{12}Co_{81}Ti_7$ (SCT) are written in abbreviated form in the table, with the nominal thickness of the respective layer given in parenthesis. Both the buffer and capping layers consist of $Al_{70}Zr_{30}$.

Sample	Thickness (nm)		
Phase/-s (nominal thickness (nm))	Buffer	Magnetic layer/-s	Capping
SCT (20)	4.6(1)	20.1(1)	4.1(1)
SCT (40)	4.6(2)	39.8(2)	4.1(1)
CAZ (40)	4.5(2)	40.2(4)	3.4(2)
SCT/CAZ/SCT (20/10/20)	4.9(1)	20.2(5)/9.5(8)/21.0(9)	3.8(1)
SCT/CAZ/SCT (20/20/20)	4.9(2)	19.4(3)/20.5(5)/20.5(3)	4.0(1)
SCT/CAZ/SCT (20/30/20)	4.7(6)	18.6(5)/30.1(6)/21.3(2)	4.7(2)
SCT/CAZ/SCT (20/40/20)	4.6(1)	19.0(4)/40.7(5)/21.0(6)	3.6(4)
SCT/CAZ/SCT (20/50/20)	4.8(1)	19.8(8)/51.0(1)/21.0(6)	4.5(3)
CAZ/SCT/CAZ (10/20/10)	4.5(1)	10.0(3)/21.05(7)/10.3(2)	4.1(1)

3. Results and discussion

3.1. Samples and structural characterisation

It was inferred from the absence of any sharp peak in the measured GI-XRD patterns that the sputtered samples are X-ray amorphous. The thickness of each individual layer in all samples are presented in Table 1.

3.2. Magnetostatic properties

The room temperature saturation magnetisation, M_s, of all samples as a function of the relative content, in vol.%, of $Sm_{12}Co_{81}Ti_7$ in the magnetic part of the film is reported in Fig. 2. These measurements are performed in-plane, using VSM. The results show a linear trend for M_s versus composition, with a decreasing saturation as the amount of $Sm_{12}Co_{81}Ti_7$ increases. The hysteresis loops from $Sm_{12}Co_{81}Ti_7$ films are isotropic, while the $Co_{85}(Al_{70}Zr_{30})_{15}$ film exhibits a clear uniaxial anisotropy. The normalised remanent magnetisation, M_r/M_s, is determined from angle dependent MOKE hysteresis loop measurements. Fig. 3 shows the resulting M_r/M_s versus in-plane measurement angle ψ_m, defined with respect to a sample edge, for the single layer $Co_{85}(Al_{70}Zr_{30})_{15}$ film of 40 nm. According to the Stoner–Wohlfarth (SW) model, valid for a single magnetic domain with uniaxial anisotropy, $M_r/M_s = |\cos(\psi)|$ where $\psi = 0°$ is the easy axis direction. Frisk et al. [30] showed that for both polycrystalline and amorphous Co-Fe-Zr films the experimental M_r/M_s versus angle

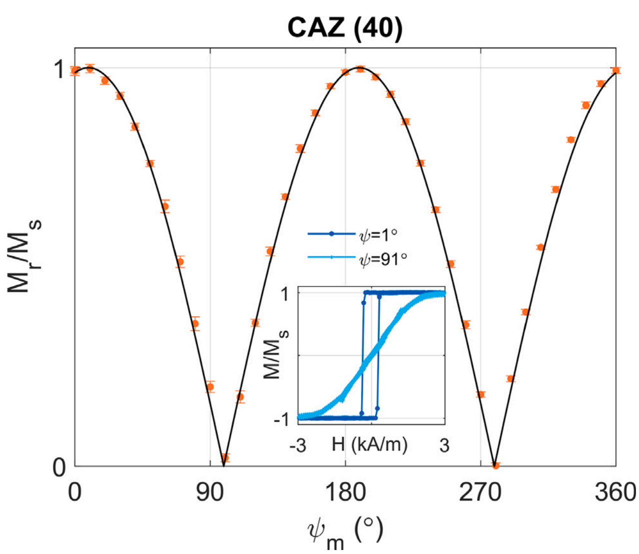

Fig. 3. MOKE measurements showing M_r/M_s versus in-plane angle ψ_m with respect to one sample edge of the 40 nm thick $Co_{85}(Al_{70}Zr_{30})_{15}$ (CAZ) sample. The fit of Eq. (1) yielding $\sigma_\psi \approx 0°$ and $\psi_0 \approx 9°$ is shown as a solid black line. Normalised hysteresis loops measured close to the easy axis ($\psi = 1°$) and close to the hard axis ($\psi = 91°$) are shown in the inset.

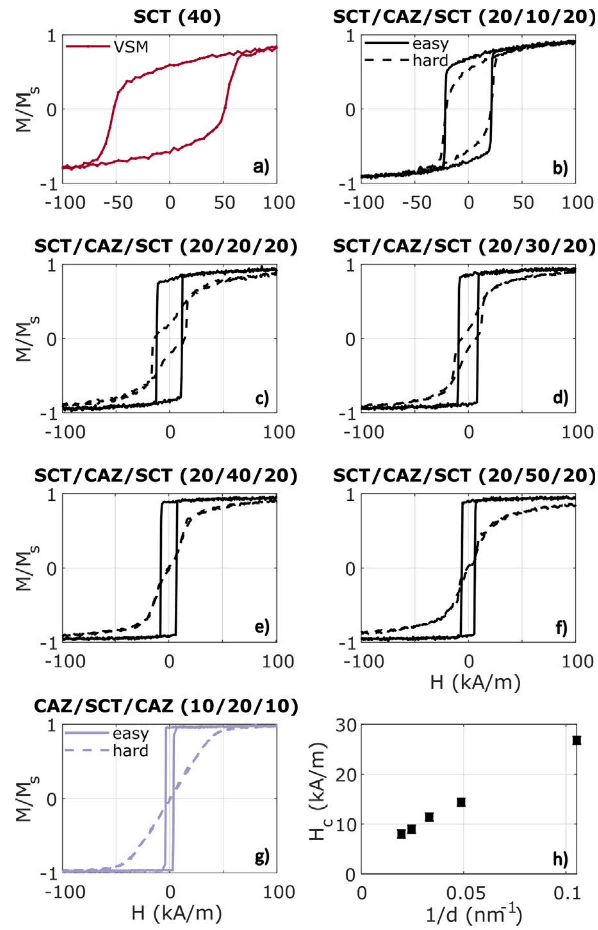

Fig. 4. (a) Normalised magnetic hysteresis loops of the $Sm_{12}Co_{81}Ti_7$ (SCT) (40) sample, measured with VSM. (b)–(f) Easy and hard axis normalised loops, measured with MOKE, for trilayers of SCT surrounding a $Co_{85}(Al_{70}Zr_{30})_{15}$ (CAZ) layer, with an increment of the CAZ layer thickness d from 10 nm up to 50 nm. (g) Corresponding MOKE data for the reverse-configuration sample, where 10 nm of CAZ surrounds 20 nm SCT. (h) Easy-axis coercivity versus the inverse CAZ layer thickness, for the trilayers with SCT/CAZ/SCT $(20/d/20)$ configuration.

behaviour is well captured by the SW model, if assuming a Gaussian distribution of easy axis directions. This behaviour would thus be exhibited by samples with multiple domains, all with uniaxial anisotropy and approximately the same easy direction and can be expressed as:

$$M_r(\psi)/M_s = \int P(\psi', \psi + \psi_0, \sigma_\psi)|cos(\psi')|d\psi', \tag{1}$$

where

$$P(\psi', \psi, \sigma_\psi) = \frac{1}{\sigma_\psi\sqrt{2\pi}} \exp\left(-\frac{(\psi' - \psi)^2}{2(\sigma_\psi)^2}\right), \tag{2}$$

σ_ψ is the width of the Gaussian distribution, and ψ' is the integration variable. Defining the measurement angle as $\psi_m = \psi + \psi_0$, the offset angle ψ_0 between the sample edge and the easy axis can in addition be determined by fitting Eq. (1) to the experimental data. This approach is applied for the 40 nm $Co_{85}(Al_{70}Zr_{30})_{15}$ film, and the fit along with the measured M_r/M_s data are shown in Fig. 3. The obtained value for the width of the distribution, $\sigma_\psi = 0.05°$, is small and has a minor impact on the fitted M_r/M_s curve compared to fixing $\sigma_\psi = 0$, hence indicating a single well-defined in-plane anisotropy axis in the sample.

The $M(H)$ loop for the 40 nm $Sm_{12}Co_{81}Ti_7$ film, shown in Fig. 4(a), is isotropic for all in-plane angles. For the trilayers of SCT/CAZ/SCT with thicknesses (20 nm/d/20 nm), the in-plane anisotropy becomes more pronounced with increasing thickness d of the $Co_{85}(Al_{70}Zr_{30})_{15}$ layer, as can be seen in Fig. 4(b)–(f), where the easy and hard axis MOKE hysteresis loops are shown. There is also a clear decrease in coercivity when d increases, as shown in Fig. 4(h). All easy axis H_c values are well below the 50 kA/m of the 40 nm thick $Sm_{12}Co_{81}Ti_7$ film, but also higher than the value $H_c = 0.3$ kA/m of the 40 nm thick $Co_{85}(Al_{70}Zr_{30})_{15}$ film (see inset of Fig. 3).

The coupling between the hard and soft phases appears to be stronger in the CAZ/SCT/CAZ (10 nm/20 nm/10 nm) trilayer, shown in Fig. 4(g), since the easy axis loop is square and saturates at lower fields compared to the SCT/CAZ/SCT (20/d/20) trilayers, while the hard axis loop is well approximated by a straight line. Selected hysteresis loops, measured with VSM, of the trilayers with equal amounts of $Co_{85}(Al_{70}Zr_{30})_{15}$ and $Sm_{12}Co_{81}Ti_7$ are shown in Fig. 5. M_r/M_s versus ψ are plotted in the insets and indicate that the anisotropy is uniaxial, as for the 40 nm thick $Co_{85}(Al_{70}Zr_{30})_{15}$ sample. The lines are fits to Eq. (1), yielding $\sigma_\psi = 0.22°$ for SCT/CAZ/SCT (20/40/20) and $\sigma_\psi =$ 0.13° for CAZ/SCT/CAZ (10/20/10). This indicates a more well-defined anisotropy easy axis for the thinner trilayer, which we relate to a stronger coupling between the hard and the soft phase in this sample, where in addition the hard phase is surrounded by the soft phase.

Since the sputtered layers are X-ray amorphous we do not expect the samples to exhibit any crystalline texture which could introduce anisotropy. As mentioned in the introduction, the origin of in-plane uniaxial anisotropy in amorphous soft magnetic layers is still not fully understood. In a recent investigation of amorphous $Co_{1-x}(Al_{70}Zr_{30})_x$ thin films [21], anisotropy is suggested to arise from substrate effects, in agreement with previous studies on other systems [17,18]. If an in-plane magnetic field is applied during growth, the $Sm_{12}Co_{81}Ti_7$ layers will also be affected [26–28]. It is interesting to note that in our sample series the magnetic anisotropy is only manifest in the presence of the soft phase, and that it increases with the soft layer thickness in the trilayers (Fig. 4). This indicates that any substrate effect causing the anisotropy has to be propagated through the 20 nm thick hard phase, which we know is isotropic from the single layer $M(H)$ measurements. Strain at the substrate-buffer interface can persist throughout the layers, but bond-orientational bulk anisotropy contributions are also possible [18]. Very careful and extensive experimental investigations are necessary to distinguish between possible mechanisms [17, 18].

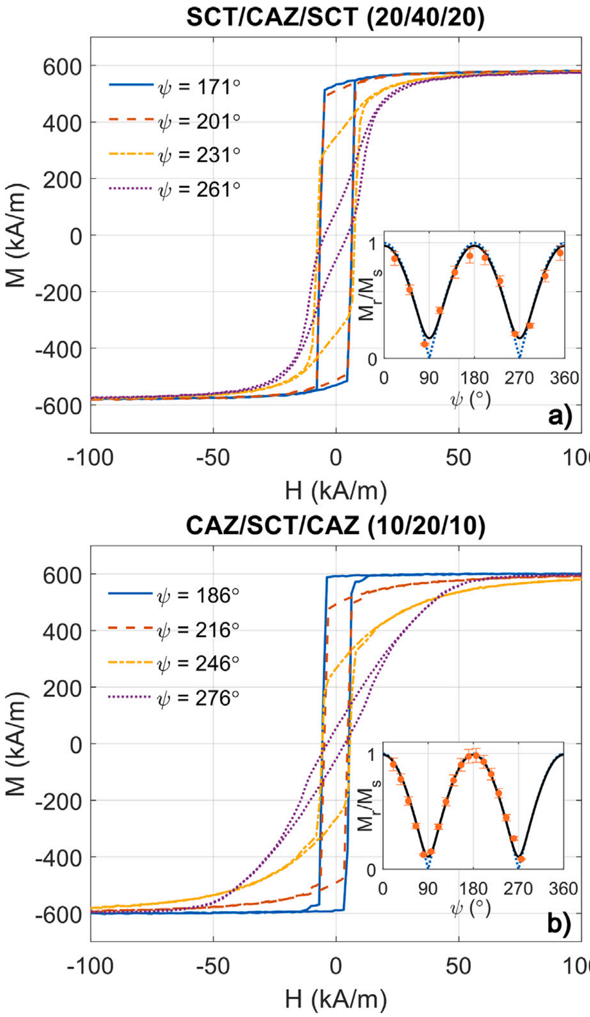

Fig. 5. In-plane M vs. H of trilayer samples of $Sm_{12}Co_{81}Ti_7$ (SCT) and $Co_{85}(Al_{70}Zr_{30})_{15}$ (CAZ) with the configuration (a) SCT/CAZ/SCT (20/40/20) and (b) CAZ/SCT/CAZ (10/20/10), where the nominal layer thicknesses in nm are given in parenthesis. The insets show M_r/M_s vs. ψ. The solid line in each inset is a fit to Eq. (1), and the dotted line is $|\cos(\psi)|$. The data is measured using VSM.

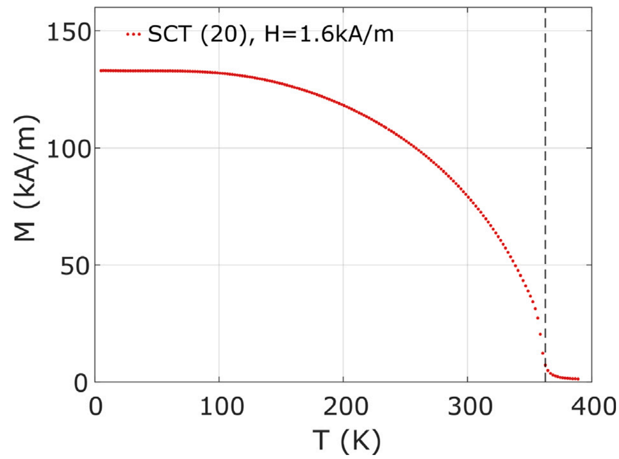

Fig. 6. Temperature dependence of the field-cooled magnetisation for the $Sm_{12}Co_{81}Ti_7$ (SCT) 20 nm thick film. The applied field is 1.6 kA/m. T_c = 363 K is shown as a black dashed line.

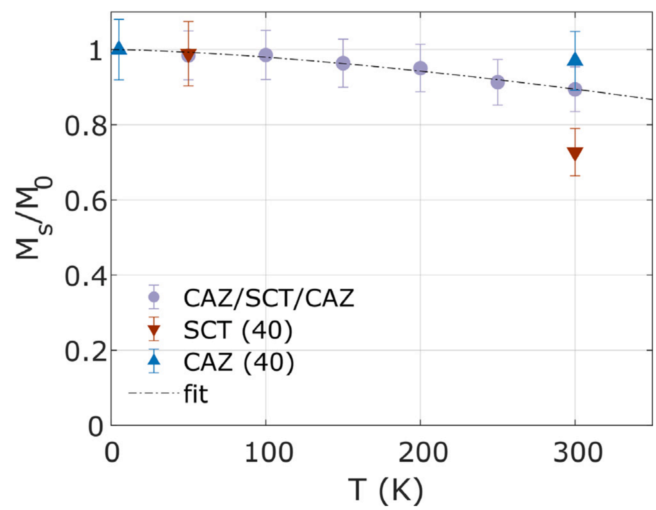

Fig. 7. M_s vs. T for the 40 nm thick $Sm_{12}Co_{81}Ti_7$ (SCT (40)) and $Co_{85}(Al_{70}Zr_{30})_{15}$ (CAZ (40)) films, and the trilayer CAZ/SCT/CAZ (10/20/10) sample. The dashed line is meant to serve as a guide for the eye and is a fit of the trilayer data in accordance with Eq. (3).

We also investigated the Curie temperatures, T_c, of the $Sm_{12}Co_{81}Ti_7$ films. For the 20 nm thick $Sm_{12}Co_{81}Ti_7$ film, T_c was determined to be 363 K, based on the minimum of the derivative from a field-cooled (FC) magnetisation measurement, with an applied field of 1.6 kA/m, shown in Fig. 6. The T_c of the thicker (40 nm) $Sm_{12}Co_{81}Ti_7$ film is above 400 K and could not be determined in an FC measurement. By extrapolating the results of Thórarinsdóttir et al. [21] we estimate T_c of amorphous $Co_{85}(Al_{70}Zr_{30})_{15}$ to be about 830 K.

The thermal behaviour of the magnetisation in ferromagnets at low temperatures, where magnon excitations dominate the reduction of the saturation magnetisation M_s at a temperature T, can be described using Bloch's power law [32]:

$$M_s(T) = M_0\left(1 - \left(\frac{T}{T_c}\right)^{\frac{3}{2}}\right), \tag{3}$$

where M_0 is the magnetisation at 0 K. This relation is used to create a guiding line in Fig. 7, indicating the qualitative relationship between the thermal stabilities of the samples, by looking at the temperature dependence of the magnetisation compared to idealised Bloch law case. In Fig. 7, M_s/M_0 is plotted versus temperature for the 40 nm thick $Sm_{12}Co_{81}Ti_7$ and $Co_{85}(Al_{70}Zr_{30})_{15}$ films as well as for the CAZ/SCT/CAZ (10/20/10) trilayer. It appears that the 40 nm $Sm_{12}Co_{81}Ti_7$ film has a significantly lower thermal stability of the saturation magnetisation than the two other samples.

4. Conclusions

Magnetic trilayer samples are studied, consisting of layers of magnetically hard $Sm_{12}Co_{81}Ti_7$ and magnetically soft $Co_{85}(Al_{70}Zr_{30})_{15}$. Saturation magnetisation is found to scale linearly with the volume fraction of $Sm_{12}Co_{81}Ti_7$. Uniaxial in-plane anisotropy is observed, from the angular dependence of remanence, in a single-layer sample of $Co_{85}(Al_{70}Zr_{30})_{15}$ and in trilayers with both phases, but not in single-layer $Sm_{12}Co_{81}Ti_7$ films. The uniaxial in-plane anisotropy inherent in the $Co_{85}(Al_{70}Zr_{30})_{15}$ layer(s) persists in the trilayers with $Sm_{12}Co_{81}Ti_7$, also with the hard/soft/hard layer configuration, and is more well defined for trilayers with thicker soft layers and if the hard layer is sandwiched in between two soft layers (soft/hard/soft configuration). Further investigation of the origins of this uniaxial anisotropy would be of interest. The coercivities of the trilayers are significantly reduced compared to the single layer of $Sm_{12}Co_{81}Ti_7$, but enhanced compared to $Co_{85}(Al_{70}Zr_{30})_{15}$. The Curie temperature, T_c, of $Sm_{12}Co_{81}Ti_7$ depends on the layer thickness and is much lower than that of $Co_{85}(Al_{70}Zr_{30})_{15}$.

CRediT authorship contribution statement

Julia Löfstrand: Formal analysis, Investigation, Writing – original draft, Writing – review & editing, Visualization. **Parul Rani:** Formal analysis, Investigation, Writing – original draft, Writing – review & editing, Visualization. **Petra E. Jönsson:** Formal analysis, Investigation, Writing – review & editing, Supervision, Funding acquisition. **Gabriella Andersson:** Conceptualization, Resources, Writing – review & editing, Supervision, Project administration, Funding acquisition.

Declaration of competing interest

The authors declare that they have no known competing financial interests or personal relationships that could have appeared to influence the work reported in this paper.

Data availability

Data will be made available on request.

Acknowledgements

Financial support by the Swedish Research Council (project grant 2017-03725) and the Swedish Energy Agency, Sweden (research project grant P48716-1) is gratefully acknowledged.

Appendix A. Supplementary data

Supplementary material related to this article can be found online at https://doi.org/10.1016/j.jmmm.2023.171186.

References

[1] F. Hellman, A. Hoffmann, Y. Tserkovnyak, G.S. Beach, E.E. Fullerton, C. Leighton, A.H. MacDonald, D.C. Ralph, D.A. Arena, H.A. Dürr, et al., Rev. Modern Phys. 89 (2017) 025006.
[2] C. Vaz, J. Bland, G. Lauhoff, Rep. Progr. Phys. 71 (2008) 056501.
[3] L. Fallarino, B.J. Kirby, E.E. Fullerton, J. Phys. D: Appl. Phys. 54 (2021) 303002.
[4] J. Jiang, J. Pearson, Z. Liu, B. Kabius, S. Trasobares, D. Miller, S. Bader, D. Lee, D. Haskel, G. Srajer, et al., J. Appl. Phys. 97 (2005) 10K311.
[5] E.F. Kneller, R. Hawig, IEEE Trans. Magn. 27 (1991) 3588.
[6] R. Skomski, J. Coey, Phys. Rev. B 48 (1993) 15812.
[7] R. Skomski, P. Manchanda, P. Kumar, B. Balamurugan, A. Kashyap, D.J. Sellmyer, IEEE Trans. Magn. 49 (2013) 3215.
[8] E.E. Fullerton, J. Jiang, M. Grimsditch, C. Sowers, S. Bader, Phys. Rev. B 58 (1998) 12193.
[9] E. Goto, N. Hayashi, T. Miyashita, K. Nakagawa, J. Appl. Phys. 36 (1965) 2951.
[10] N. De Sousa, A. Apolinario, F. Vernay, P. Monteiro, F. Albertini, F. Casoli, H. Kachkachi, D. Schmool, Phys. Rev. B 82 (2010) 104433.
[11] P.M. Monteiro, D. Schmool, Phys. Rev. B 81 (2010) 214439.
[12] P.T. Korelis, A. Liebig, M. Björck, B. Hjörvarsson, H. Lidbaum, K. Leifer, A. Wildes, Thin Solid Films 519 (2010) 404.
[13] G. Muscas, R. Brucas, P.E. Jönsson, Phys. Rev. B 97 (2018) 174409.
[14] M. Ahlberg, A. Zamani, E. Östman, H. Fashandi, B. Hjörvarsson, P.E. Jönsson, Phys. Rev. B 90 (2014) 184403.
[15] R. Alben, J.J. Becker, M.C. Chi, J. Appl. Phys. 49 (1978) 1653.
[16] G. Herzer, IEEE Trans. Magn. 26 (1990) 1397.
[17] A.T. Hindmarch, C.J. Kinane, M. MacKenzie, J.N. Chapman, M. Henini, D. Taylor, D.A. Arena, J. Dvorak, B.J. Hickey, C.H. Marrows, Phys. Rev. Lett. 100 (2008) 117201, publisher: American Physical Society.
[18] A.T. Hindmarch, A.W. Rushforth, R.P. Campion, C.H. Marrows, B.L. Gallagher, Phys. Rev. B 83 (2011) 212404, publisher: American Physical Society _eprint: 1106.0606.
[19] M. Gueye, P. Lupo, F. Zighem, D. Faurie, M. Belmeguenai, A.O. Adeyeye, Europhys. Lett. 114 (2016) 17003, publisher: EDP Sciences, IOP Publishing and Società Italiana di Fisica.
[20] M. Gueye, F. Zighem, M. Belmeguenai, M.S. Gabor, C. Tiusan, D. Faurie, J. Phys. D 49 (2016) 145003, publisher: IOP Publishing.
[21] K. Thórarinsdóttir, N. Strandqvist, V. Sigurjónsdóttir, E. Thorsteinsson, B. Hjörvarsson, F. Magnus, APL Mater. 10 (2022) 041103.
[22] Y. Suzuki, J. Haimovich, T. Egami, Phys. Rev. B 35 (1987) 2162, publisher: American Physical Society.
[23] K. Mandal, M. Vazquez, D. García, F. Castano, C. Prados, A. Hernando, J. Magn. Magn. Mater. 220 (2000) 152.
[24] H. Raanaei, H. Nguyen, G. Andersson, H. Lidbaum, P. Korelis, K. Leifer, B. Hjörvarsson, J. Appl. Phys. 106 (2009) 023918.
[25] A. Masood, P. McCloskey, C. Mathúna, S. Kulkarni, AIP Adv. 8 (2018) 056109, publisher: AIP Publishing LLC.
[26] K. Chen, H. Hegde, S.U. Jen, F.J. Cadieu, J. Appl. Phys. 73 (1993) 5923.
[27] F. Magnus, R. Moubah, A.H. Roos, A. Kruk, V. Kapaklis, T. Hase, B. Hjörvarsson, G. Andersson, Appl. Phys. Lett. 102 (2013) 162402.
[28] W. Liang, H. Zhou, J. Xiong, F. Hu, J. Li, J. Zhang, J. Wang, J. Sun, B. Shen, Engineering 6 (2020) 159.
[29] A. Frisk, The Importance of Controlling Composition to Tailor the Properties of Magnetic Thin Films (Ph.D. thesis), Acta Universitatis Upsaliensis, 2016.
[30] A. Frisk, M. Ahlberg, G. Muscas, S. George, R. Johansson, W. Klysubun, P.E. Jönsson, G. Andersson, Phys. Rev. Mater. 3 (2019) 074403.
[31] M. Björck, G. Andersson, J. Appl. Crystallogr. 40 (2007) 1174.
[32] J.M. Coey, Magnetism and Magnetic Materials, Cambridge University Press, 2010.